High saturation magnetization in $Ni_{0.2}Mn_{0.8}Fe_2O_4$ nanoparticles

D. B. Basha[a,*], E. Veena[b], M. C. Sekhar[c], A. Mallikarjuna[d], B. V. S. Reddy[e]
[a]*Department of Information Sciences, College of Computer and Information Sciences, Majmaah University, Al'Majmaah-11952, Saudi Arabia*
[b]*Department of Physics, PC Jabin Science College, Hubbali-580031*
[c]*Department of physics, Chaitanya Bharathi Institute of Technology, Hyderabad-500072, Telangana.*
[d]*Department of Physics, Audisankara College of Engineering and Technology, Gudur-524101, A.P, India*
[e]*Department of Physics, The National College, Bagepalli-561207, Karnataka, India*

The present work is focused on the synthesis of NiMn ferrite nanoparticles using hydrothermal method. The samples are examined by X-ray diffractometer (XRD), Field emission scanning electron microscope (FESEM), Transmission electron microscope (TEM), Vibrating sample magnetometer (VSM) and LCR controller in order to understand the ferrite structure, crystallite size, surface morphology, grain size, particle size, M-H loop behavior, and the variation of magnetic permeability as a function of frequency and composition. The results indicated that the high saturation magnetization is observed in case of high manganese content. Besides, the permeability versus frequency plots satisfied the Snoke's law.

(Received March 21, 2022; Accepted August 4, 2022)

Keywords: Nanoparticles, Ferrites, Surface morphology, Magnetic properties

1. Introduction

It is evidenced that the ferrites in bulk as well as nanoform established significant applications in the fields of memory devices, magnetic tapes, microwave devices, photocatalytic, antimicrobial, transformer & inductor cores, antenna, magnetic hyperthermia, electromagnetic shields etc., [1-8]. The efficient of these applications is a dependent of type substituent/dopant, cationic distribution, spinel structure, and kind of synthesis technique [9-14]. It is a known fact that the ferrites will have a general chemical formula: AFe_2O_4 (where 'A' tends to divalent metal ions such as Ni. Mg, Cu, Zn, Mn, etc) [15-17]. It is commonly considered as magnetic spinel structure. These spinels are classified into three types such as normal spinel, inverse spinel, and mixed spinel. This is done based on the degree of inversion (δ) of spinel structure. That is, δ =1 for normal spinel, δ =0 for inverse spinel, and δ=0.25 for mixed spinel [18]. These structures of ferrites vary from bulk to nano. For example, nickel ferrite shows inverse spinel structure in bulk form occupying the nickel ions octahedral and tetrahedral sites equally. On the other hand, the same ferrite reveals the mixed spinel structure in nanoform [18].

The nickel ferrite is extensively studied for various applications in the field of science and technology in bulk and nanoform [18]. Many scientists worked on nickel ferrite to report the structural, electrical, optical, magnetic, microwave, electromagnetic, biomedical etc., properties. For instance, the literature [1-18] shows that several scientists worked on nickel ferrite, and its based bulk, and nanoferrites to investigate the structure, particle size, surface morphology, electrical, dielectric, magnetic, electromagnetic, microwave, and optical properties. Similarly, the PVDF/$NiFe_2O_4$ based electrospun nanofibers are synthesized for flexible piezoelectric nanogenerators [19], the cytotoxicity of nickel ferrite nanocomposite [20], nickel ferrite nanospheres [21], the electromagnetic wave absorber nature of honeycomb-like $NiFe_2O_4$@Ni@C

* Corresponding author: b.dudekula@mu.edu.sa
https://doi.org/10.15251/JOR.2022.184.591

composites [22], nickel ferrite showing the anti-angiogenic activity [23], the $NiFe_2O_4$-Zn-Al mixed metal oxide composite shows the synergistic photocatalytic-adsorption removal effect [24], the nickel ferrite is developed via the optimization of porous structure as high sensitivity acetone sensor [25], the wide band electromagnetic wave absorber is developed from $NiO/NiFe_2O_4$@N-doped reduced graphene oxide aerogel [26], the preparation of imines/benzothiazoles/benzoxazoles from nitroarenes using nano-nickel ferrite as catalyst under microwave irradiation [27], the efficient supercapacitors are developed by $NiFe_2O_4/SiO_2$ nanostructures [28], the water splitting agent is produced using ultrathin carbon coated mesoporous Ni-$NiFe_2O_4$ nanosheet arrays [29], lomefloxacin is degraded using $NiFe_2O_4$/CuS activator [30], $SnO_2/NiFe_2O_4$ nanocomposites developed for studying magnetic, and optical properties [31], nickel ferrite nanoparticles are prepared using green fabrication for non-enzymatic determination of pentachlorophenol [32], the emerging technological applications are acquired by rare earth doped nickel ferrite nanocomposite [33], $NiFe_2O_4$ & NiO@$NiFe_2O_4$ nanoparticles are synthesized for supercapacitors [34], multi wall carbon promoted nickel ferrite is produced for synergistic catalytic degradation of ciprofloxacin [35], nickel based nanosheet with spinel nickel ferrite is prepared for nanoflower composite catalyst [36], anticancer, and antibiotic activities are achieved due to lime peel extract induced nickel ferrite nanoparticles [37], the $NiFe_2O_4$/CdO p-n nano-heterojunctions are developed for solar light activated photodegradation of methylene blue dye applications [38], and the high-performance nano-electrocatalyst in alkaline media is prepared from hydrazine on $NiFe_2O_4$-rGO [39]. From the vast literature survey, it is concluded that many nickel ferrite-based reports are seen, and the reports on Mn doped nickel ferrite nanoparticles are very limited. Hence, the authors considered to synthesize nano NiMn ferrites via hydrothermal technique due to its low temperature, high crystallinity, homogeneity, less cost, and easy synthesis [18]. Therefore, the NiMn ferrites are prepared with varying composition from 0.2 to 0.8. Further, samples are studied for various characterizations using the XRD, FESEM, TEM, VSM, and LCR controller for investigating the structural, morphological, and magnetic behavior of samples.

2. Experimental procedure

We selected the raw materials like nickel nitrate, manganese nitrate, iron nitrate, and NaOH pellets for the synthesis of nano NiMn ferrites. At the outset, the nitrate materials are dissolved in distilled water and stirred for half an hour. The solution is further shifted to a fresh glass beaker and kept on a stirrer with hotplate. The mixture is stirred and, in the meantime, the NaOH solution is added. As a result, the pH of the resultant solution reaches 11. As mentioned in the literature [18], the ferrite compound will be formed successfully. Further, the solution is shifted to Teflon bowl of 300 ml capacity, and it is kept in stainless steel autoclave. The whole autoclave is kept in hot air oven to perform hydrothermal reaction. The reaction is carried out at 180^{o}C for 6 hours. After completion of reaction, the oven is cooled to room temperature. Then, the solution is removed from Teflon bowl and shifted to fresh glass beaker. The water content is removed by the centrifuge and drying process. As a result, the fine powder is developed which is called as nano NiMn ferrite.

3. Results and discussion

Fig.1 shows the X-ray diffraction patterns of NiMn ferrite nanoparticles. It is seen that the x = 0.2-0.8 samples indicated the formation of single-phase cubic spinel structure. Hence, it is understood that the produced samples are of pure in nature. The good crystallinity is developed for all samples. The maximum intensity is recorded at the reflection plane (311) for all ferrite nanoparticles. The diffraction peaks are in good agreement with the standard JCPDS card No.:86-2267. This evidenced a fact that the structure of Ni-ferrite is remained unaltered upon doping the Mn-element. Furthermore, the lattice parameters are calculated using the formula: $a=b=c= d*[h^2+k^2+l^2]^{0.5}$, where hkl are the Miller indices, ‘d’ is the interatomic distance, and a, b & c are the lattice constants [18]. The results revealed a fact that the lattice constants are increasing from

0.8382 to 0.8729 nm as a function of ‘x’. This kind of results is attributed to the ionic radii effect in the spinel ferrite system. That is, Mn^{2+} cations show the tetrahedral ionic radii: 0.0655 nm & octahedral ionic radii: 0.080 nm, while the Ni^{2+} ions will have tetrahedral ionic radii: 0.055 nm & octahedral ionic radii: 0.069 nm [40, 41]. This shows that the Mn^{2+} ions have greater ionic radii than Ni^{2+} ions. As a result, the unit cell will be expanded leading to the increase of lattice constants with increase of Mn-content. This follows Vegard’s law (see Fig.2) [41]. Further, the average crystallite size (D) is determined using Scherrer relation: $D=0.9\lambda/\beta\cos\theta$, where ‘β’ is the full width half maxima, and ‘θ’ is the angle of diffraction [18]. The obtained results expressed that the ‘D’ value is varying from 36 to 72 nm as a function of ‘x’. The ‘D’ value is increased due to the high ionic radii of manganese cations.

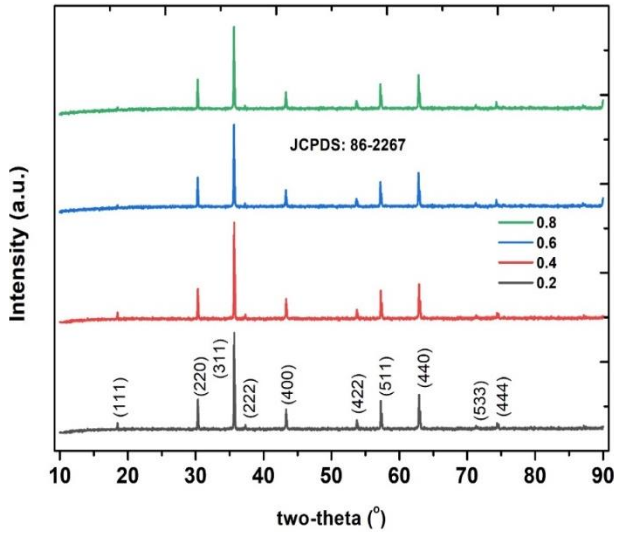

Fig. 1. XRD patterns of NiMn ferrite nanoparticles.

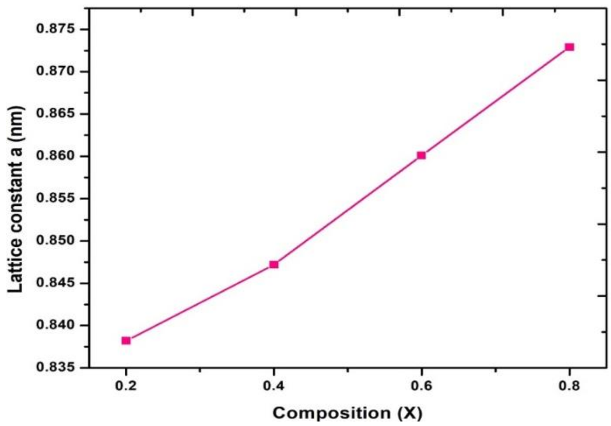

Fig. 2. Variation of lattice parameter of NiMn ferrite nanoparticles.

Table 1. Data on structural & morphological parameters of NiMn ferrite nanoparticles.

x	0.2	0.4	0.6	0.8
Crystallite size D (nm)	36.3	49.2	64.4	72.1
a/b/c (nm)	0.8382	0.8472	0.8601	0.8729
Particle size P (nm)	38.4	46.2	57.2	62.5
Grain size G (nm)	149.1	154.4	163.8	171.4

In Fig. 3, the FESEM pictures are shown indicating the clustered like grains. The average grain size is found to be changing from 149 to 171 nm with ‘x’. This size is given directly from the FESEM machine itself. Herein, the similar increasing trend of grain size is noticed as in case of crystallite size. The samples indicated the existence of grains attached to each other. This behavior is due to the high magnetic interactions of nanoparticles. The shape of grains seems to be asymmetrical spheres with increase of Mn-content. Besides, the TEM pictures shown in Fig.4 indicates the similar clustered like asymmetrical spheres. The presence of nanoparticles is evidenced from the TEM pictures. The average particle size is increased from 38 to 62 nm as a function of ‘x’ (Table.1). These results are in consistent with the variation trend of crystallite size, and grain size with Mn-content.

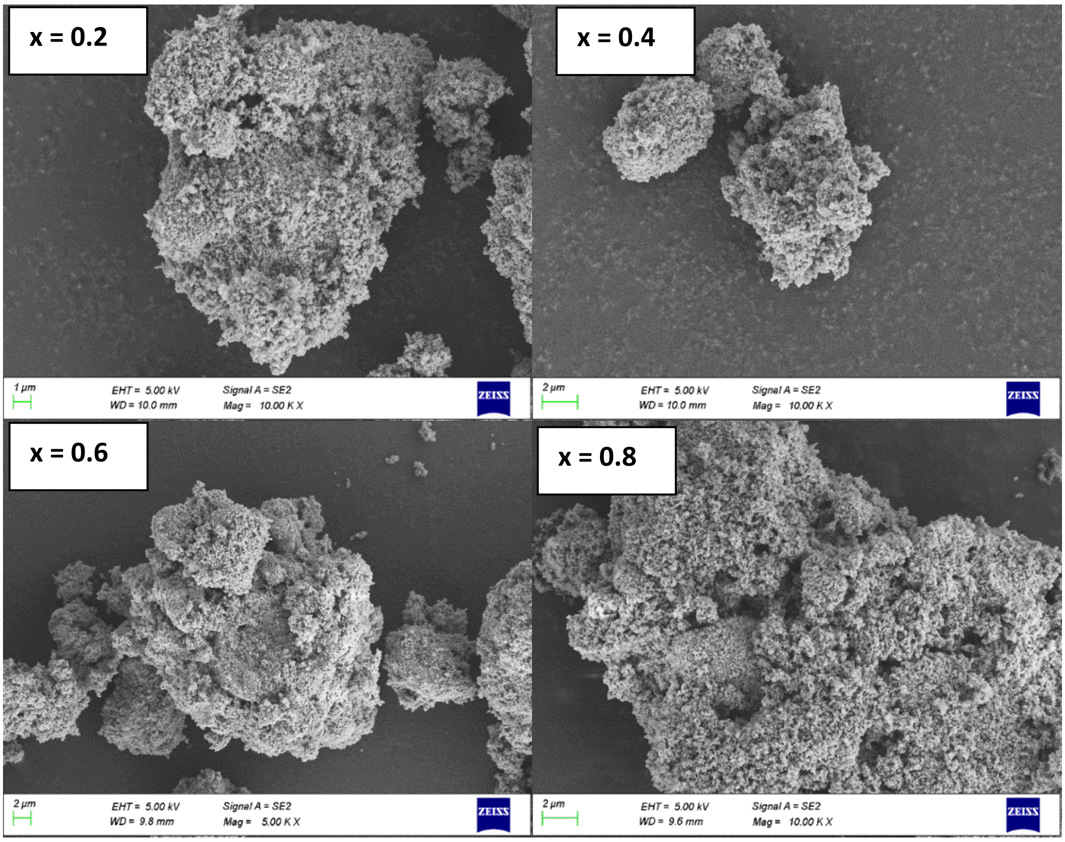

Fig. 3. FESEM pictures of NiMn ferrite nanoparticles.

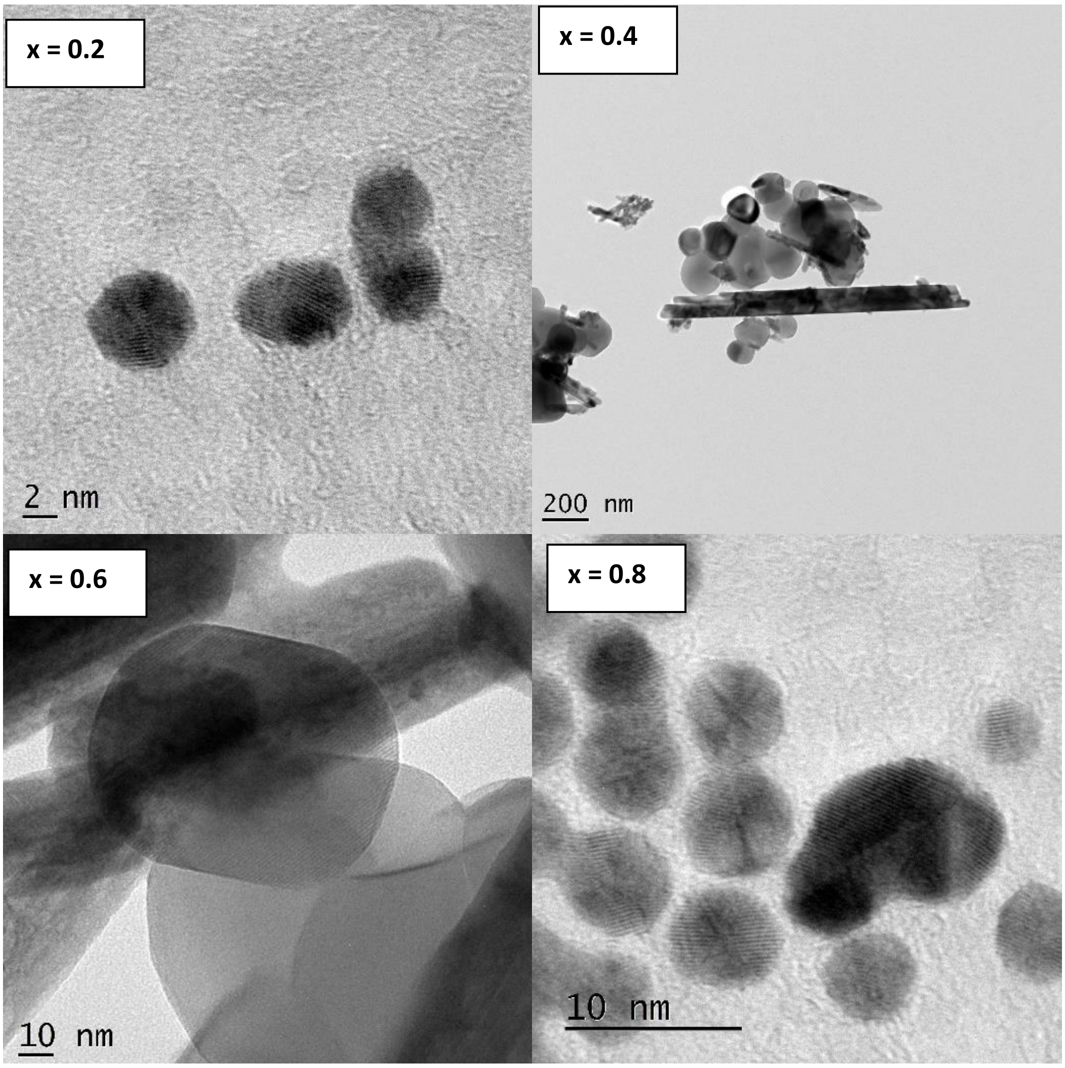

Fig. 4. TEM pictures of NiMn ferrite nanoparticles.

The magnetic permeability (μ_i) versus frequency plots of x=0.2-0.8 samples are depicted in Fig.5. It is noticed that the permeability of all samples is almost constant at lower frequencies. This trend is started at 100 Hz and continued up to 50 kHz. For further increase of frequency, the permeability plots show the falling nature of μ_i value at 0.1 MHz. This establishes a fact that the NiMn ferrite nanoparticle obey Snoke's law [16]. For all the samples, it is noticed at 1 MHz frequency. This kind of trend is observed due to the matching of input magnetic field frequency with the spinning magnetic dipoles. Once, it is happened, the resonance will be taken place. As a result of the resonance, the permeability goes to maximum (due to high agitation in the magnetic dipoles), and suddenly falls down. The sharp falling of curves indicates the high homogeneity of prepared samples. In addition, compositional dependence of permeability shows the unsystematic variation. This is attributed to the variation of ferric ions at the octahedral (B) sites. Further, the M-H loops (Fig.6) are recorded and show that the saturation magnetization is increased with Mn-content. This is basically the high magnetic moment of Mn^{+2} ions with 6 μB as compared with Ni^{2+} ions with 3 μB. Moreover, the larger number of Mn^{2+} ions occupy the B-site rather than the tetrahedral (A) site. As we know that the high number of magnetic cations at the B-site usually induce the magnetic moment. Thus, it leads to the increase of predominant magnetization with increase of Mn-content (see Fig.7). The loops are seemed to be having small loop area indicating the soft magnet behavior of NiMn ferrite nanoparticles. It is seen that the saturation magnetization (M_s) of ferrites started from 52.69 emu/g, and ended with 87.15 emu/g. This clearly indicated the increase of even saturation magnetization which is due to higher concentration of magnetic cations at the B-site. Furthermore, the cation distribution is performed using the M-H loop data. It is mentioned in Table.2. It is observed that the Mn^{2+} cations and Ni^{2+} cations are shifted to B-site. Thus, according to two-sublattice model, the resultant magnetic moment $M=M_B-M_A$, will be very high. It is clearly seen in the cation distribution.

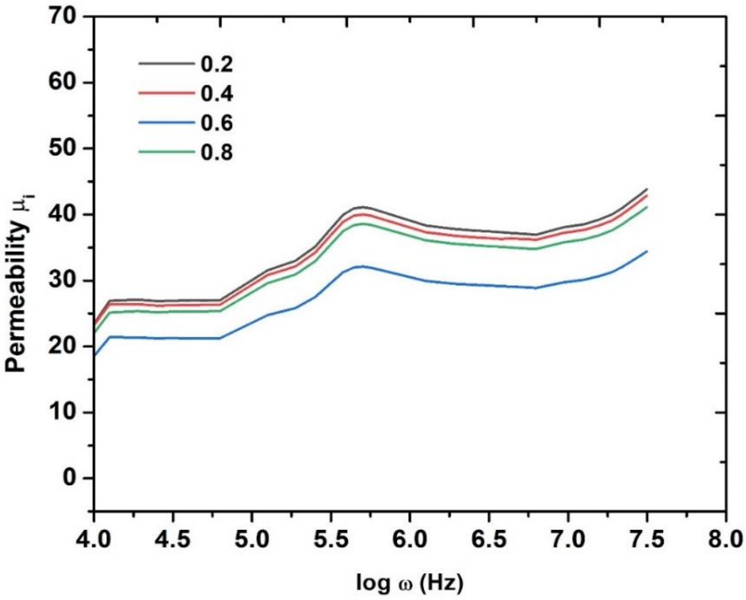

Fig. 5. Frequency dependence of permeability of NiMn ferrite nanoparticles.

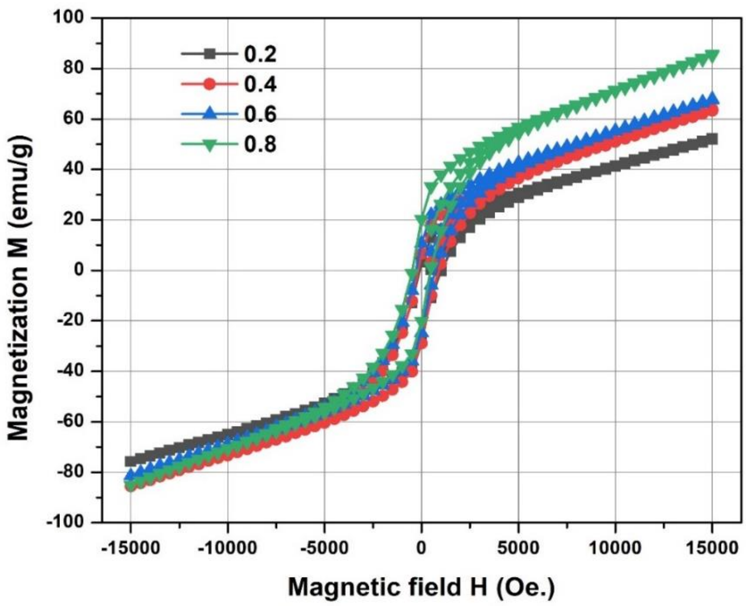

Fig. 6. M-H loops (hysteresis) of NiMn ferrite nanoparticles.

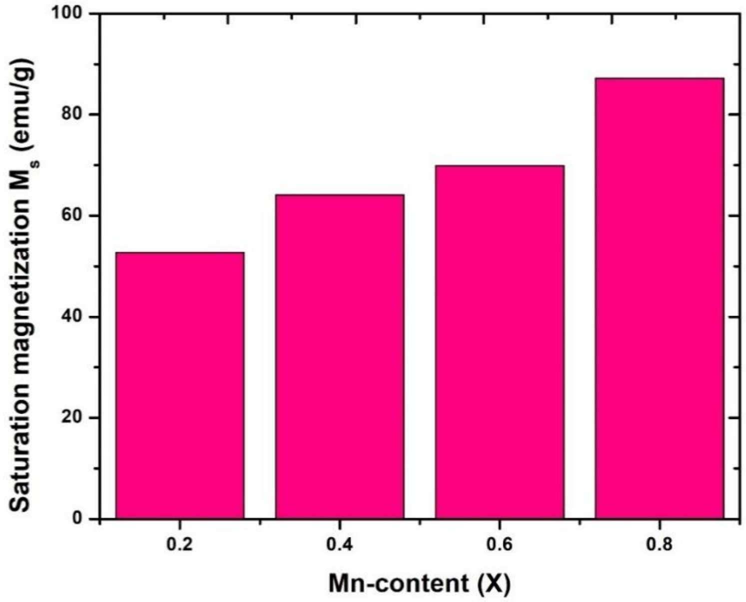

Fig. 7. Compositional dependence of M_s of NiMn ferrite nanoparticles.

Table 2. Cation distribution of NiMn ferrite nanoparticles.

x	A-site			B-site		
	Ni^{2+}	Mn^{2+}	Fe^{3+}	Ni^{2+}	Mn^{2+}	Fe^{3+}
0.2	0.2	0.05	0.95	0.4	0.15	1.05
0.4	0.25	0.1	0.95	0.15	0.3	1.1
0.6	0.2	0.2	0.85	0.2	0.4	1.15
0.8	0.1	0.25	0.75	0.1	0.55	1.25

4. Conclusions

The NiMn ferrites with x=0.2-0.8 in nanoform are prepared using hydrothermal method. The cubic structure is confirmed by XRD patterns. The lattice constants are noticed to be increasing from 0.8382 to 0.8729 nm as a function of ‘x’. The FESEM and TEM pictures showed the asymmetrical nanospheres with high agglomeration due to magnetic interactions. The frequency dependence of magnetic permeability of present samples shows the Snoke’s limit at 0.1 MHz indicating the decrease of permeability. The M-H loops reveal the highest saturation magnetization for x=0.8 composition with a value of 87.15 emu/g.

Acknowledgements

The author D.Baba Basha would like to thank the Deanship of Scientific Research at Majmaah University for supporting this work under Project Number No. R-2022-241

References

[1] T.V. Sagar, T.S. Rao, K.C.B. N, Mater. Chem. Phys. 258, 123902 (2021); https://doi.org/10.1016/j.matchemphys.2020.123902

[2] T. Vidya Sagar, T. Subba Rao, K.C.B. N, Ceramic International (2020); https://doi.org/10.1016/j.ceramint.2020.01.178

[3] Abdul Gafoor, K.C.B. N, D. Ravinder, Khalid Mujasam Batoo, Syed Farooq Adil, Mujeeb Khan, Applied Physics A, 2019; https://doi.org/10.1007/s00339-019-3225-1

[4] Nehru Boda, K.C.B. N, Khalid Mujasam Batoo, G. Helen Ruth Joice, J. Laxman Naik, Dachepalli Ravinder, Biointerface Research in Applied Chemistry 10 (2020) 4752-4763; https://doi.org/10.33263/BRIAC101.752763

[5] U. Naresh, R. J. Kumar, K.C.B. N, Ceramics International 45 (2019) 7515-7523; https://doi.org/10.1016/j.ceramint.2019.01.044

[6] Nehru Boda, K.C.B. N, D. Baba Basha, D. Ravinder, Journal of Superconductivity and Novel Magnetism (2019); https://doi.org/10.1007/s10948-019-05242-1

[7] N. Boda, G. Boda, K.C.B. N, M. Srinivas, K. M. Batoo, D. Ravinder, A.P. Reddy, Journal of Magnetism and Magnetic Materials, 473 (2019) 228-235; https://doi.org/10.1016/j.jmmm.2018.10.023

[8] U. Naresh, R. J. Kumar, K.C.B. N, Materials Chemistry and Physics 236 (2019)121807; https://doi.org/10.1016/j.matchemphys.2019.121807

[9] Vinuthna C H, K. K.C.B. N, Chandra Sekhar C, Ravinder D, International Journal of Applied Ceramic Technology, 2019; https://doi.org/10.1111/ijac.13276

[10] K.C.B. N, N. S. Kumar & G. Ranjith Kumar & S. Naresh Kumar, Journal of Australian Ceramic Society 55 (2019) 541-548; https://doi.org/10.1007/s41779-018-0260-x

[11] K.C.B. N and W. Madhuri, IEEE Transactions on Magnetics 54 (2018), 2300808; https://doi.org/10.1109/TMAG.2018.2855663

[12] T. Ramaprasad, R. J. Kumar, U. Naresh, M. Prakash, D. Kothandan, K.C.B. N, Materials Research Express 5 (2018) 095025; https://doi.org/10.1088/2053-1591/aad860

[13] K.C.B. N and W. Madhuri, Materials Chemistry and Physics 187 (2017) 164-176; https://doi.org/10.1016/j.matchemphys.2016.11.062

[14] K.C.B. N, S. Roopas Kiran and W. Madhuri, IEEE Transactions on Magnetics 53 (2017) 2900207; https://doi.org/10.1109/TMAG.2016.2625773

[15] K.C.B. N and W. Madhuri, Materials Chemistry and Physics 181; https://doi.org/10.1016/j.matchemphys.2016.06.079

[16] K.C.B. N and W. Madhuri, International Journal of Applied Ceramic Technology 13 (2016) 1090-1095; https://doi.org/10.1111/ijac.12571

[17] K.C.B. N & Madhuri Wuppulluri, Phase Transitions 90 (2017) 847-862; https://doi.org/10.1080/01411594.2016.1277220

[18] K.C.B. N and W. Madhuri, Bulletin of Materials Science 40 (2017) 417-425; https://doi.org/10.1007/s12034-017-1374-4

[19] Levent Paralıa, Çiğdem Elif, Demirci Dönmezb, Muhterem Koçc, Selçuk Aktür, Current Applied PhysicsVolume 36, April 2022, Pages 143-159; https://doi.org/10.1016/j.cap.2022.01.013

[20] Egizbek, K.; Kozlovskiy, A.L.; Ludzik, K.; Zdorovets, M.V.; Korolkov, I.V.; Marciniak, B.; M, Jazdzewska; Chudoba, D.; Nazarova, A.; Kontek, R. (2020). Stability and cytotoxicity study of NiFe2O4 nanocomposites synthesized by co-precipitation and subsequent thermal annealing. Ceramics International, (), S0272884220308683-. doi:10.1016/j.ceramint.2020.03.222 https://doi.org/10.1016/j.ceramint.2020.03.222

[21] Alyami, B. A., Mahmoud, A. M., Alkahtani, S. A., & El-Wekil, M. M. (2021), Talanta, 226, 122167; https://doi.org/10.1016/j.talanta.2021.122167

[22] Zhixin Liu, Yiqun Wang, Zirui Ji, Mingbo Ling, Yonglie Yan, Liang Chai, Haiying Du,

Guanglei Wu, Journal of Colloid and Interface ScienceVolume 608, Part 3, 15 February 2022, Pages 2849-2859; https://doi.org/10.1016/j.jcis.2021.11.012

[23] Santos, J. G., Lopes, H., Moreno, H., Ramirez, M. A., Garcia, F. G., & Simões, A. Z. (2021). Ceramics International, 47(11), 16152-16161; https://doi.org/10.1016/j.ceramint.2021.02.191

[24] Veisi, P., Seyed Dorraji, M. S., Rasoulifard, M. H., Ghaffari, S., & Khobkar Choobar, A. (2021), Journal of Photochemistry and Photobiology A: Chemistry, 414, 113268; https://doi.org/10.1016/j.jphotochem.2021.113268

[25] Zhang, Sufang; Jiang, Wenhao; Li, Yiwen; Yang, Xueli; Sun, Peng; Liu, Fangmeng; Yan, Xu; Gao, Yuan; Liang, Xishuang; Ma, Jian; Lu, Geyu (2019), Sensors and Actuators B: Chemical, S0925400519306136; https://doi.org/10.1016/j.snb.2019.04.090

[26] Qijie Wang, Junnan Wang, Yazhen Zhao, Yu Zhao, Junfeng Yan, Zhouhu Deng, Han Zhang, Wu Zhao, JiangxiaoTian, Jiangni Yun, Zhiyong Zhang, Zhiwei Huang, Chemical Engineering Journal Volume 430, Part 2, 15 February 2022, 132814l https://doi.org/10.1016/j.cej.2021.132814

[27] Patel, G., Patel, A. R., Lambat, T. L., & Banerjee, S. (2021), Current Research in Green and Sustainable Chemistry, 4, 100149; https://doi.org/10.1016/j.crgsc.2021.100149

[28] Baig, M. M., Pervaiz, E., Azad, M., Jahan, Z., Khan Niazi, M. B., & Baig, S. M. (2021), Ceramics International, 47(9), 12557-12566; https://doi.org/10.1016/j.ceramint.2021.01.113

[29] Zhang, Jianfang; Jiang, Ying; Wang, Yan; Yu, Cuiping; Cui, Jiewu; Wu, Jingjie; Shu, Xia; Qin, Yongqiang; Sun, Jian; Yan, Jian; Zheng, Hongmei; Zhang, Yong; Wu, Yucheng (2019). Electrochimica Acta, (), 134652; https://doi.org/10.1016/j.electacta.2019.134652

[30] Xinyi Zhang, Yingjie Gao, Yunhe Li, Yuerong Zhou, Haiyan Ma, Jiangwei Shang, Xiuwen Cheng, Separation and Purification Technology Volume 288, 1 May 2022, 120664; https://doi.org/10.1016/j.seppur.2022.120664

[31] El Desouky, Fawzy G.; Saadeldin, M.M.; Mahdy, Manal A.; El Zawawi, I.K. (2020), Vacuum, (), 110003; https://doi.org/10.1016/j.vacuum.2020.110003

[32] Syed Iqleem, H. Taqvia. Amber R. Solangi, Jamil A Buledib, Nadir H. Khand, Bindia Junejo Almas, F. Memona, Sidra Ameenc, Atiya Bhattib, Pau-Loke Showd, Yasser Vasseghiane, Hassan Karimi-Maleh, Chemosphere Volume 294, May 2022, 133760; https://doi.org/10.1016/j.chemosphere.2022.133760

[33] Majid Niaz, Akhtara Muhammad, Yousaf Yuzheng, Luc Mustafa, Z. Mahmoudde, Javed Iqbal, Muhammad Azhar, Khang Muhammad, Umar Khallidoonh, Sami Ullahi, Mohamed Hussien, Synthetic MetalsVolume 284, March 2022, 116994; https://doi.org/10.1016/j.synthmet.2021.116994

[34] Zhang, Y., Zhang, W., Yu, C., Liu, Z., Yu, X., & Meng, F. (2021), Ceramics International, 47(7), 10063-10071; https://doi.org/10.1016/j.ceramint.2020.12.153

[35] Alireza Badi, Sarac Eslam, Ghareh Shabania, Mohammad Haghighi, Maryam Shabani, Journal of the Taiwan Institute of Chemical EngineersVolume 132, March 2022, 104131; https://doi.org/10.1016/j.jtice.2021.10.031

[36] Yeqing Zhang, Lei Ye, Meilin Zhang, Lufang Ma, Yaqiong Gong, Applied Surface Science, 2022, 152957; https://doi.org/10.1016/j.apsusc.2022.152957

[37] Abdul Raouf, Malika Muhammad, Hammad Aziz, Muhammad Atif, Muhammad Sultan Irshad, Hafeez Ullah, Tuan Nguyen Gia, Hijaz Ahmed, Shafiq Ahmad, Thongchai Botmart, Journal of Saudi Chemical SocietyVolume 26, Issue 2, March 2022, 101422; https://doi.org/10.1016/j.jscs.2022.101422

[38] Philips O. Agboola, Imran Shakir, Sajjad Haider, Ceramics InternationalAvailable online 25 January 2022; https://doi.org/10.1016/j.ceramint.2022.01.236

[39] Mohammad Bagher, Askaria Parisa Salarizadeh, Hadi Beitollahi, Somayeh Tajik, Abolfath Eshghi, Sadegh Azizi, Materials Chemistry and PhysicsVolume 275, 1 January 2022, 125313; https://doi.org/10.1016/j.matchemphys.2021.125313

[40] Qiang-min, Wei Jian-biao, Li Yong-jun, Chen Yong-sheng, Han, Materials Characterization Volume 47, Issues 3-4, September-October 2001, Pages 247-252; https://doi.org/10.1016/S1044-5803(01)00177-2

[41] Abid Hussain, Tahir Abbas, Shahida B. Niazi, Ceramics InternationalVolume 39, Issue 2, March 2013, Pages 1221-1225; https://doi.org/10.1016/j.ceramint.2012.07.049